Characteristics, sources, and reactions of nitrous acid during winter at an urban site in the Central Plains Economic Region in China

Qi Hao, Nan Jiang*, Ruiqin Zhang, Liuming Yang, and Shengli Li

Key Laboratory of Environmental Chemistry and Low Carbon Technologies of Henan Province, Research Institute of Environmental Science, College of Chemistry, School of Ecology and Environment, Zhengzhou University, Zhengzhou 450001, China

Abstract

Nitrous acid (HONO) in the core city of the Central Plains Economic Region was measured using an ambient ion monitor from January 9 to 31, 2019. Measurement time intervals were classified into the following periods in accordance with the daily mean values of $PM_{2.5}$: clean days (CD), polluted days (PD), and severely polluted days (SPD). The HONO concentrations during CD, PD, and SPD were 1.2, 2.3, and 3.7 ppbv, respectively. The contribution of the homogeneous reaction, heterogeneous conversion, and direct emission to HONO sources varied under different pollution levels. The mean values of the net HONO production of the homogeneous reaction (P_{OH+NO}^{net}) in CD, PD, and SPD periods were 0.13, 0.26, and 0.56 ppbv h^{-1}, respectively. The average conversions of NO_2 (C_{HONO}) in CD, PD, and SPD periods were 0.72×10^{-2}, 0.64×10^{-2}, and 1.54×10^{-2} h^{-1}, respectively, indicating that the heterogeneous conversion of NO_2 was unimportant than the homogeneous reaction. Furthermore, the net production of the homogeneous reaction may have been the main factor for the increase in HONO under high-NO_X conditions (i.e., when the concentration of NO was higher than that of NO_2) at nighttime. Daytime HONO budget analysis showed that the mean values of the unknown source ($P_{unknown}$) during CD, PD, and SPD periods were 0.26, 0.40, and 1.83 ppbv h^{-1}, respectively. The values of P_{OH+NO}^{net}, C_{HONO}, and $P_{unknown}$ in the SPD period were comparatively larger than those in other periods, indicating that HONO participated in many reactions. The proportions of nighttime HONO sources also changed during the entire sampling period. Direct emission and a

heterogeneous reaction controlled HONO production in the first half of the night and provided a contribution larger than that of the homogeneous reaction. The proportion of homogenization gradually increased in the second half of the night due to the steady increase in NO concentration. The hourly level of HONO abatement pathways, except for OH + HONO, was at least 0.22 ppbv h^{-1} in the SPD period. The cumulative frequency distribution of the HONO$_{emission}$/HONO ratio (less than 20%) was approximately 77%, which suggested that direct emission was not important. The heterogeneous HONO production increased when the relative humidity (RH) increased, but it decreased when RH increased further. The average HONO/NO$_X$ ratio (4.9%) was more than twice the assumed globally averaged value (2.0%).

1. Introduction

Nitrous acid (HONO) is important in the photochemical cycle and can provide hydroxyl radicals (OH) (Harrison et al., 1996):

$$HONO + hv \rightarrow \cdot OH + NO \ (300 \text{ nm} < \lambda < 405 \text{ nm}) \tag{R1}.$$
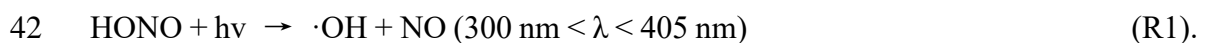
According to measurement and simulation studies (Alicke et al., 2002), the contribution of HONO to ·OH concentration can reach 25−50%, especially when the concentration of OH radicals produced by the photolysis of ozone, acetone, and formaldehyde is relatively low (two to three hours after sunrise) (Czader et al., 2012). HONO photolysis was the most important primary source of ·OH which contributed up to 46 % of the total primary production rate of radicals for daytime conditions (Tan et al., 2018). ·OH is an important oxidant in the atmosphere, and it can react with organic substances, control the oxidation capacity of the atmosphere, and accelerate the formation of secondary aerosols in the urban atmosphere (Sörgel et al., 2011). Therefore, the changes in the contribution of the homogeneous reaction, heterogeneous conversion, and direct emission during pollution can be observed by studying the formation mechanism of HONO.

Several instruments have been used to determine ambient HONO concentrations, and these include differential optical absorption spectrophotometer (DOAS)

2

(Elshorbany et al., 2012; Winer and Biermann, 1994), long path absorption photometer (LOPAP) (Heland et al., 2001), wet chemical derivatization technique-HPLC/UV-Vis detection (Michoud et al., 2014), stripping coil-UV/Vis absorption photometer (SC-AP) (Pinto et al., 2014), IBBCEAS (Duan et al., 2018; Min et al., 2016), CIMS (Hirokawa et al., 2009; Roberts et al., 2010), and ambient ion monitor (AIM) (VandenBoer et al., 2014). A result comparison of different instruments showed that SC-AP is compatible with two spectral measurement instruments, namely, LOPAP and DOAS (Pinto et al., 2014). Compared with HONO measured by SC-AP deployed onsite, HONO measured by AIM has a small error and is within the acceptable analytical uncertainty (VandenBoer et al., 2014). Previous studies have reported that HONO concentrations range from a few pptv in clean remote areas to several ppbv (0.1−2.1 ppbv) in air-polluted urban areas (Hou et al., 2016; Michoud et al., 2014).

The sources of HONO are direct emission and homogeneous and heterogeneous reactions (Acker et al., 2005; Grassian, 2001; Kurtenbach et al., 2001). HONO can be directly discharged into the atmosphere during vehicle operation and biomass combustion. Through a tunneling experiment, Kurtenbach et al. (2001) have discovered that motor vehicles emit a small amount of HONO, and the HONO/NO_X ratio of HONO combustion sources (aside from NO_X and other pollutants) is 0.1–0.8%. Another study showed that the homogeneous reaction of NO and OH radicals is the major source of HONO under increased NO concentrations (Spataro et al., 2013). Furthermore, HONO can react with the ·OH (Alicke, 2003; Vogel et al., 2003). Tong et al. (2015) used NO + OH and HONO + OH homogeneous reactions, to calculate the net generation rate of HONO homogeneous reactions at night, which are expressed as:

$$NO + \cdot OH \; \rightarrow \; HONO \qquad\qquad\qquad (R2);$$

$$HONO + \cdot OH \; \rightarrow \; NO_2 + H_2O \qquad\qquad\qquad (R3).$$

Such calculations have been applied in studies on homogeneous reactions and daytime budgets (Hou et al., 2016; Huang et al., 2017). These are studies of homogeneous reactions, and some researchers have begun to explore the mechanism of NO_2

85 heterogeneous reactions. Finlayson-Pitts et al. (2003) studied the mechanism of

86 chemical adsorption of NO_2 and H ions on the adsorbed surface was revealed by using

87 isotope-labeled water:

88 $2NO_2 + H_2O \rightarrow HONO + HNO_3$ (R4).

89 In China, most studies for HONO have concentrated on the Yangtze River Delta, Pearl

90 River Delta, and Jing-Jin-Ji region. For example, Hao et al. (2006) reported that field

91 measurement results, especially $HONO/NO_2$ and relative humidity (RH), have a

92 significant correlation and proved that heterogeneous reactions are an important source

93 of nighttime HONO. Although the specific chemical mechanisms of heterogeneous

94 reactions remain unknown, the intensity of HONO formation by NO_2 can be expressed

95 by the HONO conversion frequency (Alicke et al., 2002; Li et al., 2012). Su et al.

96 (2008a) revealed the importance of the ·OH from HONO during daytime (9:00–15:00

97 local time) and found that many unknown sources which are closely related to the solar

98 radiation leading to HONO formation. The unknown sources of HONO may include

99 the NO_2 photolysis of sooty surface and adsorbed nitric acid and nitrate at UV

100 wavelengths (Kleffmann et al., 1999). The homogeneous nucleation of NO_2, H_2O, and

101 NH_3 is the HONO formation pathway (Zhang and Tao, 2010). In the meanwhile, HONO

102 can deposit and react with amines in forming nitrosamines (Li et al., 2012) for sinking.

103 The method of budget analysis needs to include the HONO sources and sinks. The

104 researchers suggested that the method of budget analysis is crucial for obtaining the

105 missing source. Spataro et al. (2013) measured the HONO level in Beijing's urban area

106 and discussed the spatiotemporal changes, meteorological effects, and contributions of

107 HONO from different sources. They used the measured HONO data to compare

108 pollution periods in Beijing's urban and suburban areas. Tong et al. (2015) discovered

109 that the pathway of the HONO formation mechanism, namely, direct emission,

110 heterogeneous formation, and homogeneous reaction is the same, but the pathway is

111 different in the two sites. A few studies (Cui et al., 2018; Hou et al., 2016) compared

112 the characteristics and sources of HONO during severe-pollution and clean periods.

113   Although the definitions of the two periods are different, both can be used to analyze

114   the diurnal variation, source, and daytime budget of HONO during the aggravation of

115   pollution.

116   There is no study of HONO in the Central Plains Economic Region (CPER), with

117   a total population of 0.18 billion by the end of 2011. CPER is the important region for

118   food production and modern agriculture published by the Chinese government

119   (http://www.gov.cn/zhengce/content/2011-10/07/content_8208.htm).   The   file

120   described the different factors which affect atmospheric pollution, including the level

121   of economic development, energy structure, industrial structure and geographical

122   location (solar radiation) with the Yangtze River Delta, Pearl River Delta, and Jing-Jin-

123   Ji region. As the core city of CPER, Zhengzhou characterized by severe PM (particulate

124   matters) pollution (Jiang et al., 2018b), is selected in the study. In recent years,

125   comprehensive PM research has been conducted on the chemical characteristics of PM

126   in Zhengzhou (Li et al., 2019), source apportionment (Liu et al., 2019), health risks

127   (Jiang et al., 2019), and emission source profiles (Jiang et al., 2018a). However, no

128   study has been performed on the sources and characteristics of HONO in Zhengzhou.

129   Moreover, no synthetic research on different pollution levels in the area is available. In

130   the current study, AIM was used to sample and analyze HONO concentrations. The

131   interactions between HONO and other factors, such as $PM_{2.5}$, during pollution, were

132   assessed to understand the formation and removal of HONO and the influence on

133   different pollution periods. The levels of $PM_{2.5}$ were divided into three periods to

134   analyze the HONO sources, sinks, and reactions in different periods. Many papers

135   (Huang et al., 2017; Tong et al., 2016) took $PM_{2.5}$ as the main control factor of HONO, and

136   studied the differences of HONO sources and characteristics between clean and polluted

137   periods. No homogeneous reaction, direct emission, heterogeneous reaction, and daytime

138   budget analysis were conducted during the period of worsening pollution (namely HD period

139   in this paper). Total NO_X emissions in cities with different leading factors of emissions

140   have been declining year by year due to Chinese government emission control measures,

141 but some Chinese cities are still in high-NO_X areas (e.g. Beijing, Shanghai, Guangzhou

142 and Zhengzhou.) (Kim et al., 2015; Liu et al., 2017). Under high-NO_X conditions, some

143 papers (Cui et al., 2018; Hou et al., 2016) suggested that heterogeneous reaction was

144 the main source of HONO and did not conduct a quantitative analysis of homogeneous

145 reaction, especially in winter. So, we explore relevant studies of homogeneous reactions.

146 In addition, the source contributions of HONO at night varied with the degree of

147 pollution level were not explained. RH was also analyzed to provid a detailed

148 understanding of HONO generation intensity under different RH conditions. Analysis

149 of the sources of HONO at night provides strong support for conducting HONO budget

150 analysis during daytime. To the best of the authors' knowledge, the formation

151 characteristics of HONO at continuous and high time resolutions and different pollution

152 levels have not been studied in Zhengzhou. This work can assist the governments of the

153 CPER in formulating policy to decrease the level of HONO precursors, i.e., NO and

154 NO_2, and HONO direct emission from the vehicle.

2. Experiment and methods

2.1. Sampling site and period

157 The sampling site is on the rooftop (sixth floor) of a building in Zhengzhou

158 University (34°48' N, 113°31' E), which is located in the northwestern part of

159 Zhengzhou, China. The observation height is about 20 m from the ground, and the

160 observation platform is relatively open without any tall buildings around. The site is

161 about 500 m from the western Fourth-Ring Expressway of Zhengzhou City and about

162 2 km from Lian Huo Expressway to the north. The measurement period was from

163 January 9 to 31, 2019. Daily data were divided into two periods, namely, daytime (7:00–

164 18:00 local time) and nighttime (19:00–6:00 the next day, LT).

2.2. Instruments

166 AIM (URG-9000D, Thermo, USA), an online ion chromatographic monitoring

167 system for particle and gas components in the atmosphere, was used to measure HONO

168 concentration continuously at a temporal resolution of 1 h. The atmospheric airflow

169 entered the $PM_{2.5}$ cyclone cutting head through the sample tube, and gas–solid

170 separation was performed with a parallel plate denuder with a new synthetic polyamide

171 membrane. The denuder had no moving parts and could be changed without stopping

172 the sampler. HONO was absorbed by the denuder with an absorption liquid (5.5 mM

173 H_2O_2). The chemicals that could be oxidized were absorbed by H_2O_2 on the porous

174 membrane surface, but several gases (e.g., O_2 and N_2) were expelled by the air pump.

175 The abundance of other gaseous acids and bases affected the efficiency of HONO

176 collection by AIM due to the relation between Henry's law constant and pH. This

177 measurement method and its details have been successfully evaluated in many field

178 studies (Markovic et al., 2012; Tian et al., 2018; Wang et al., 2019), and shown in the

179 supplement. In addition, a QXZ1.0 automatic weather station (Yigu Technologies,

180 China) was used for synchronous observation of meteorological parameters, including

181 temperature (T), RH, wind direction (WD), and wind speed (WS). A temporal

182 resolution of the model analyzer (TE [used for measuring O_3], 48i [used for measuring

183 CO], 42i [used for measuring NO, NO_X, and NO_2], and TEOM 1405 $PM_{2.5}$ monitor

184 [used for measuring $PM_{2.5}$], Thermo Electron, USA) is 1 h. Detailed information can

185 be found in the work of (Wang et al., 2019). Measurement technique, detection limit,

186 and accuracy of measured species are shown in **Table S1**.

187   During the sampling period, all instruments were subjected to strict quality control

188 to avoid possible contamination. The instrument accessories and sampling process were

189 periodically replaced and calibrated, respectively. The instrument parts and

190 consumables were changed before the observation process, and the sampling flow was

191 calibrated to reduce the negative effect of accessories. Before this measurement period,

192 the membrane of the denuder has been replaced and standard anion and cation solutions

193 have been prepared on Jan. 3rd. The standard curve should be drawn to ensure the

194 appropriateness of the correlation coefficient ($\geqslant$ 0.999) and the accuracy of the sample

195 retention time and response value. The minimum detection limit of AIM was 0.004

196 ppbv. Other detailed information can be found in the work of (Wang et al., 2019).

3. Results and Discussion

3.1. Temporal variations of meteorological parameters and pollutants

The daily changes in meteorological parameters and $PM_{2.5}$ are shown in **Fig. 1**. In accordance with the daily average concentration level of $PM_{2.5}$, the analysis and measurement process was divided into three periods (clean days [CD], polluted days [PD], and severely polluted days [SPD]). The days wherein the daily averages of $PM_{2.5}$ were lower than the daily average of second grade in China National Ambient Air Quality Standards (CNAAQS) ($75\ \mu g\ m^{-3}$) represented CD (January 9, 16, 17, 21, 22, 23, 26, and 31), with RH ranging from 5 to 79% and WS ranging from 0 to $4.2\ m\ s^{-1}$. The days wherein the daily averages of $PM_{2.5}$ were between 75 and $115\ \mu g\ m^{-3}$ represented PD (January 10, 15, 18, 20, 25, 27, and 28), with RH ranging from 17 to 86% and WS ranging from 0 to $4.6\ m\ s^{-1}$. The days wherein the daily averages of $PM_{2.5}$ were higher than $115\ \mu g\ m^{-3}$ represented SPD (January 11, 12, 13, 14, 19, 24, 29 and 30), with RH ranging from 30 to 96% and WS ranging from 0 to $3.5\ m\ s^{-1}$. Northwest or east wind was observed in most of the observation periods, except for January 21–22. WD was north, the maximum WS reached 4 m/s, the $PM_{2.5}$ concentration decreased rapidly, and the effect of pollutant removal was evident. **Table 1** lists the data statistics of HONO, $PM_{2.5}$, NO_2, NO, NO_X, $HONO/NO_2$, $HONO/NO_X$, O_3, CO, T, RH, WS, and WD during the measurement period together with their mean value ± standard deviation. The meteorological parameters in **Table 1** show that the average RH in CD, PD, and SPD periods was 33, 49, and 68%, respectively. In SPD, RH was high and WD was low (mean value of $0.4\ m\ s^{-1}$).

In accordance with the data on trace gases, the average HONO values in CD, PD, and SPD were 1.1, 2.3, and 3.7 ppbv, respectively. The mean values of NO_2 were 25, 33, and 42 ppbv (46, 63, and 78 $\mu g\ m^{-3}$ lower than the first grade in CNAAQS [80 μg m^{-3}]), respectively. The mean values of CO were 1, 1, and 2 ppmv (1, 2, and 2 $mg\ m^{-3}$ lower than the first grade in CNAAQS [4 $mg\ m^{-3}$]), respectively. **Fig. 2** shows the concentration changes in HONO and gas species throughout the measurement period.

The variations of the average HONO, $PM_{2.5}$, NO_2, and CO in the three periods were similar. The mean values of all pollutant concentrations except O_3 in the SPD period were the largest, and those in the CD period were the smallest. The highest mean value of O_3 occurred in the CD period, similar to previous observations (Hou et al., 2016; Huang et al., 2017; Zhang et al., 2019).

The HONO concentrations ranged from 0.2 to 14.8 ppbv and had an average of 2.5 ppbv, which is higher than the average values of 0.6 (Rappenglück et al., 2013), 1.5 (Hou et al., 2016), and 1.0 ppbv (Huang et al., 2017) in previous urban studies. The diurnal variations of HONO during the measurement were similar in the three periods, as shown in **Fig. 3** and **Fig. 4**. The diurnal variations of HONO, NO, NO_2, O_3, HONO/NO_2, and HONO/NO_X are illustrated in **Fig. 4**. The error bars of **Fig. 4** were placed separately in the tables of the supplement (**Table S2**). After sunset, the HONO concentrations in CD, PD, and SPD began to accumulate due to the attenuation of solar radiation and the stabilization of the boundary layer (Cui et al., 2018). The maximum values of 1.7, 4.1, and 6.9 ppbv were reached in the morning (08:00–10:00 LT) in CD, PD, and SPD, respectively. After 10:00 LT, the HONO concentration decreased because of the increased solubility and rapid photolysis, remaining at a low level before sunset (14:00–16:00 LT). The NO concentration decreased rapidly in the forenoon, and remained low in the afternoon. After sunset, the concentrations of NO and NO_2 began to increase and remained at a higher level than the daytime. Furthermore, the diurnal variation of NO in the CD period was similar to that of NO_2. The peak was reached at around 09:00 LT due to vehicle emission in the morning rush hours, and the lowest value was observed at around 16:00 LT. After 18:00 LT, the boundary layer height decreased in the evening rush hours, resulting in an increase in NO and NO_2 concentrations (Hendrick et al., 2014). O_3 showed a diurnal cycle and had maximum values in CD, PD, and SPD periods in the afternoon. The HONO/NO_2 ratio is commonly used to estimate the formation of HONO in NO_2 transformation (Wang et al., 2013). Compared with HONO formation, NO_2 transformation is less affected by the

253   migration of atmospheric airmass during atmospheric migration (Li et al., 2012). The

254   HONO/NO$_2$ ratio in the CD period began to increase after sunset and reached its peak

255   at night. Then, it decreased in the morning as a result of the enhancement of NO$_2$

256   emission and photolysis of HONO. However, the mean value of HONO/NO$_2$ in PD and

257   SPD periods gradually increased from nighttime and eventually reached the maximum

258   values of 14.3 and 18.9% at 09:00 and 10:00 LT, respectively. The average HONO/NO$_X$

259   ratio (4.9%) was more than twice the assumed globally averaged value (2.0%)

260   (Elshorbany et al., 2014). This result indicates that the strength of the heterogeneous

261   reaction increased slightly with the exacerbation of pollution. The HONO/NO$_2$ ratio

262   showed a diurnal cycle with a low level in the afternoon and a high level after sunset

263   due to the heterogeneous reaction of NO$_2$ on the ground and aerosol surface (Su et al.,

264   2008b). For comparison, the daytime and nighttime HONO, HONO/NO$_2$, and

265   HONO/NO$_X$ mean values in other cities around the world are listed in **Table 2**. The

266   values of HONO, HONO/NO$_2$, and HONO/NO$_X$ in Zhengzhou are relatively higher

267   than those in other parts of the world. The reason for this phenomenon is that

268   Zhengzhou is a high-NO$_X$ area which provides HONO with abundant precursors (NO$_2$

269   and NO) in winter (Kim et al., 2015).

270 **3.2. Nocturnal HONO sources and formation**

271 **3.2.1. Homogeneous reaction of NO and OH**

272   The homogeneous reaction of NO and OH (R2 and R3) is the main pathway of

273   HONO formation in the gas phase. Spataro et al. (2013) found that the formation

274   mechanism leads to an increase in HONO in high-pollution areas with an increase in

275   NO at night. P_{OH+NO}^{net} can be understood as the net hourly HONO production amount

276   of homogeneous reaction and is calculated as

277     $P_{OH+NO}^{net} = k_{OH+NO} [OH][NO] - k_{OH+HONO} [OH][HONO]$ (1).

278   At T = 298 K and P = 101 kPa, the rate constants of k_{OH+NO} and $k_{OH+HONO}$ are

279   9.8×10^{-12} and 6.0×10^{-12} molecule cm^{-3}, respectively (Atkinson et al., 2004; Sander et

280   al., 2003). [OH] is the concentration of ·OH that was not measured during the campaign.

Therefore, Tan et al. (2018) found that by the field measurement, the average concentration of ·OH in Beijing at nighttime was about 2.5×10^5 molecule cm^{-3}. Moreover, the same ·OH concentration was also used to calculate the homogeneous reaction of HONO in the recent researches of Beijing (Zhang et al., 2019), Shanghai (Cui et al., 2018), and Xi'an (Huang et al., 2017). And, nighttime OH concentration increased as the latitude decreases ranged 3 to 6×10^5 molecule cm^{-3} (Lelieveld et al., 2016). Zhengzhou has a lower latitude than Beijing, so the concentration of OH used in this study is 2.5×10^5 molecule cm^{-3}. P_{OH+NO}^{net} primarily depends on the concentrations of NO and HONO because the reaction rates of k_{OH+NO} and $k_{OH+HONO}$ are close. **Fig. 5** shows the nocturnal variations of P_{OH+NO}^{net}, NO, and HONO during CD, PD, and SPD periods. The error bars of **Fig. 5** were placed separately in the tables of the supplement (**Table S3**). When the NO levels were high, the variations of P_{OH+NO}^{net} followed those of NO during the three periods (Atkinson et al., 2004). The mean value of P_{OH+NO}^{net} was 0.33 ppbv h^{-1}, and the specific values in CD, PD, and SPD periods were 0.13, 0.26, and 0.56 ppbv h^{-1}, respectively. We assumed $\pm$ 50% ·OH values to estimate the uncertainty of P_{OH+NO}^{net}. The ·OH values of 1.25×10^5 and 3.75×10^5 molecule cm^{-3} were calculated the P_{OH+NO}^{net} values of 0.16 and 0.49 ppbv h^{-1}.

P_{OH+NO}^{net} varied from 0.01 to 0.47 ppbv h^{-1} during the CD period. The mean value of P_{OH+NO}^{net} increased before midnight, decreased after midnight, and increased slightly at 3 am. In the PD period, P_{OH+NO}^{net} ranged from 0.07 to 0.44 ppbv h^{-1}. The situation was similar to that in the CD period, except that the value remained almost constant. In addition, the contribution of HONO from homogeneous reaction during the SPD period was larger than those in the CD and PD periods, and the level of P_{OH+NO}^{net}, with an average value of 0.56 ppbv h^{-1}, was lower than the value in a previous study (2.18 ppbv h^{-1} in Beijing) (Tong et al., 2015). From 19:00 LT to 03:00 LT, the mean value of P_{OH+NO}^{net} increased from 0.15 to 0.9 ppbv h^{-1}. HONO increased from 2.84 to 4.59 ppbv and subsequently decreased to 4.43 ppbv. By integrating P_{OH+NO}^{net} during the eight hours, the homogeneous reaction can provide an accumulated HONO formation of at

309 least 3.36 ppbv (i.e., $0.15 + 0.20 + 0.25 + 0.25 + 0.35 + 0.56 + 0.7 + 0.9$ ppbv). However,

310 the mean accumulation value of measured HONO in this nighttime period was merely

311 1.59 ppbv. With the increase in pollution level, the HONO accumulation period at

312 nighttime increased. This result indicates that first, the homogeneous reaction of OH +

313 NO is sufficient to augment HONO in the first half of the night, although NO_2

314 transformation and other sources may still exist. When the concentration of NO is

315 relatively high, the net production generated by OH + NO may be the leading factor for

316 the increase in HONO at night (Tong et al., 2015). Second, the hourly level of HONO

317 abatement pathways, except OH + HONO, should be at least 0.22 ppbv h^{-1} (i.e., 3.36 –

318 1.59 ppbv)/8 h). This phenomenon may arise because the dry deposition on ground

319 surfaces can be the main HONO removal pathway at night, similar to a previous study

320 (Li et al., 2012).

321 **3.2.2. Direct emission**

322   At present, no HONO emission inventory or emission factor database for

323 Zhengzhou is available. As a result, estimating any HONO from direct emission is

324 difficult. In the current study, directly emitted HONO could have been generated by

325 vehicle exhaust and biomass combustion because the site is close to the western Fourth-

326 Ring Expressway of Zhengzhou City and about Lian Huo Expressway to the north.

327 Hence, only night data (17:00–06:00 LT) were considered to avoid the problem of

328 instant photolysis of directly emitted HONO. In a previous study, the $HONO/NO_X$ ratio

329 from tunnel measurement was set to 0.65% to estimate an upper limit of HONO emitted

330 by traffic near the site (Kurtenbach et al., 2001). The minimum value of $HONO/NO_X$

331 in the SPD period in the current work was 1.5%, which is slightly higher than the value

332 measured in the abovementioned study. Directly emitted HONO at night was not

333 transformed immediately. The HONO concentrations corrected by direct emissions are

334 given as

335     $[HONO]_{correct} = [HONO] - [HONO]_{emission} = [HONO] - 0.0065 \times [NO_X]$ (2),

336 where $[HONO]_{emission}$, $[NO_X]$, and 0.0065 are direct emission HONO concentration,

337 NO$_X$ concentration, and HONO/NO$_2$ direct emission ratio, respectively. The direct

338 emission contribution was estimated by comparing the direct emission HONO with the

339 observed HONO. The ranges of HONO$_{emission}$/HONO in CD, PD, and SPD periods were

340 2–52%, 6–34%, and 2–41%, respectively, and the mean values were 17, 16, and 16%,

341 respectively. The frequency distribution of the HONO$_{emission}$/HONO ratio at nighttime

342 is shown in **Fig. 6**. For this upper limit estimation, the frequency distribution of

343 HONO$_{emission}$/HONO (less than 20%) was approximately 77%. Hence, direct emission

344 may not be the main reason for the high growth of HONO levels. Compared with the

345 direct emission of other sites, that of the measurement site accounted for a lower

346 proportion possibly because the site is relatively far from the highway on the campus.

347 **3.2.3. Heterogeneous conversion of NO$_2$ to HONO**

348   NO$_2$ is an important precursor for HONO formation. In addition, recent

349 field measurements in many urban locations have shown that a positive

350 correlation exists between HONO and NO$_2$ (Cui et al., 2018; Hao et al.,

351 2006; Huang et al., 2017; Zhang et al., 2019), suggesting they have a

352 common source. Moreover, Acker et al. (2005) reported that different

353 meteorological conditions may lead to significant differences in the

354 relationship between the source and receptor, and these differences lead to

355 various types of correlation. During the measurement period, the

356 HONO/NO$_2$ ratio varied between 1.3 and 59.0%, with an average of 7.6%,

357 which is slightly higher than the 6.2% average in a previous study (Cui et

358 al., 2018). The HONO/NO$_2$ ratio calculated in this work is much larger than

359 that calculated for direct emission (< 1%) (Kurtenbach et al., 2001), suggesting

360 that heterogeneous reactions may be a more important pathway for HONO

361 production than direct emissions. With regard to the heterogeneous

362 conversion of NO$_2$, several studies (An et al., 2012; Shen and Zhang, 2013)

363 have reported that the surface of soot particles is the medium of NO$_2$

364 conversion. The contribution of soot surface to HONO production is usually

much lower than expected because the uptake efficiency of NO_2 decreases with the prolonged reaction time caused by surface deactivation. The aerosol surface is an important medium for the heterogeneous transformation from NO_2 to HONO (Liu et al., 2014). The mass concentration of aerosols was used as an alternative to identify the influence of aerosols in this study because the surface density of aerosols could not be obtained.

The correlations between $PM_{2.5}$ and $HONO/NO_2$ ratio in CD, PD, and SPD periods are shown in **Fig. 7**. With the exacerbation of the $PM_{2.5}$ level, the average value of $HONO/NO_2$ gradually increased, indicating that the aerosol surface occupied an important position in the heterogeneous transformation. A comparison of $HONO/NO_2$ and HONO with $PM_{2.5}$ showed that the correlation between $HONO/NO_2$ and $PM_{2.5}$ ($R^2 = 0.23$) was weaker than that between HONO and $PM_{2.5}$ ($R^2 = 0.55$) in the entire period. The main source of HONO could not have been the transformation of NO_2. Notably, the HONO correlation in the PD period was significantly stronger than that in the two other periods. This result proves that HONO-related reactions occurred more frequently during this period. The fair correlation between HONO and $PM_{2.5}$ may pinpoint the mainly anthropogenic origins of these two pollutants with the high direct or indirect contribution of combustion sources. The reason for the increased HONO during the heavy pollution period could be by the comparatively high loading and large particle surface (Cui et al., 2018). Similar phenomena have been observed in a correlation study on CO and HONO wherein CO was used as a tracer for traffic-induced emissions and tested by considering the correlation between HONO and CO over an identical time interval (Qin et al., 2009). The correlation coefficient between HONO and CO was relatively moderate ($R^2 = 0.43$), indicating that HONO and CO could come from the same source of emissions. Generally speaking, CO and

NO are mainly related to combustion processes such as vehicle emissions, fossil fuel and biomass combustion (Tong et al., 2016). Thus, fossil fuel and biomass combustion may contribute to HONO production, but they can not be measured directly.

The absorbed water influenced the heterogeneous formation (Stutz et al., 2004). The influence of RH on the heterogeneous conversion is shown in **Fig. 7(d)**. When RH was less, the $HONO/NO_2$ ratio slowly increased. When RH was increased, the $HONO/NO_2$ ratio began to increase rapidly with RH. The $HONO/NO_2$ ratio decreased when RH reached a certain high level. Similar variation patterns have been obtained in previous studies (Huang et al., 2017; Qin et al., 2009; Tong et al., 2015). Surface adsorbed water functions not only as sources but also as sinks of HONO by affecting the hydrolysis of NO_2 and the sedimentation of HONO to generate HONO (Ammann et al., 1998). When RH ranged at the middle level, the heterogeneous conversion of NO_2 to HONO was more significant than that of deposition. This phenomenon confirms that RH improved the conversion efficiency (Stutz et al., 2004). However, the surface reached saturation when RH reached a certain high level. The excess water restricted NO_2 transformation (Wojtal et al., 2011). The absorption and dissolution of HONO by the saturated surface water layer caused $HONO/NO_2$ ratio to decrease drastically.

The correlation between $HONO_{correct}$ and NO_2 at nighttime is shown in **Fig. S1**. $HONO_{correct}$ was used in the calculation to exclude the influence of direct emission on NO_2 conversion. The nocturnal variations of $HONO_{correct}$, NO_2, and $HONO_{correct}/NO_2$ ratios in the CD, PD, and SPD periods are presented in **Fig. 8**. The error bars of **Fig. 8** were placed separately in the tables of the supplement (**Table S4**). In general, the $HONO_{correct}/NO_2$ ratio reached its maximum at or before midnight but decreased after midnight. In the PD and

SPD periods, HONO was generated by heterogeneous reaction (R4), and NO$_2$ decreased after midnight. The production of HONO was equal to its loss (mainly night deposition), and HONO concentration reached a relatively s In the current study, directly emitted HONO state (Stutz, 2002). The weak correlation between nighttime HONO/NO$_2$ and PM$_{2.5}$ can be reasonably explained by the stable HONO$_{correct}$/NO$_2$ ratio after midnight (Qin et al., 2009). A previous study (Xu et al., 2015) found that a low HONO$_{correct}$ in the first half of the night (19:00–00:00 LT) indicates an important contribution of automobile exhaust emissions, and a low HONO$_{correct}$ in the second half of the night means heterogeneous reactions dominate. Therefore, the heterogeneous reaction conversion rate of HONO was calculated in the current study by using the data of HONO$_{correct}$.

The conversion rate of HONO (C$_{HONO}$) is usually used as an indicator to test the efficiency of NO$_2$ heterogeneous reactions. Total HONO$_{correct}$ was assumed to be generated by the heterogeneous transformation of NO$_2$. The formula for the conversion rate of NO$_2$ (C$_{HONO}$) is as follows (Su et al., 2008a; Xu et al., 2015):

$$C_{HONO} = \frac{([HONO_{correct}]_{t2} - [HONO_{correct}]_{t1}}{(t2 - t1)\,[NO_2]} \tag{3},$$

where [NO$_2$] is the average concentration of NO$_2$ within the t2–t1 time interval (1 h). In this study, the averaged conversion rate of NO$_2$ was 1.02×10^{-2} h^{-1}. The mean values of C$_{HONO}$ in the CD, PD, and SPD periods were 0.72×10^{-2}, 0.64×10^{-2}, and 1.54×10^{-2} h^{-1}, respectively. The averaged conversion rates in this study were 0.58×10^{-2} and 1.46×10^{-2} h^{-1} higher than those of Beijing I (polluted) and II (heavily polluted) periods, respectively. The increase in the conversion rate demonstrates that NO$_2$ had high reaction efficiency through the process from NO$_2$ to HONO in the aggravation of pollution, which could have led to the high utilization efficiency of the aerosol surface. The exact uptake coefficients of NO$_2$ on ground and aerosol surfaces

are variable and should be different (Harrison and Collins, 1998). The present analysis simplified this process by treating the ground and aerosol surfaces the same. The uptake coefficient is mainly dependent on the surface characteristics, e.g. surface type and moisture (Lu et al., 2018).

3.3. Daytime HONO budget

The expression of $d\,HONO\,/\,d\,t$ represents the observed variations of hourly HONO concentrations, for which we can use $\Delta\,HONO/\Delta\,d\,t$ instead:

$$d\,HONO\,/\,d\,t = sources - sinks$$

$$= (P_{unknown} + P_{OH+NO} + P_{emi} + P_{het}) - (L_{OH+HONO} + L_{photo}) \tag{4},$$

$$P_{OH+NO} = k_{OH+NO}\,[OH]\,[NO] \tag{5},$$

$$L_{OH+HONO} = k_{OH+HONO}\,[OH]\,[HONO] \tag{6}.$$

The $d\,HONO\,/\,d\,t$ calculated from the measurements was small and evenly distributed around zero (Li et al., 2012). $P_{unknown}$ is the production rate by an unknown daytime HONO source. P_{OH+NO} is the rate of reaction of NO and OH. P_{emi} represents the direct emission rate of HONO from combustion processes. By studying the source and reduction, the daytime HONO budget was analyzed with Eq. (4) (Su et al., 2008b). The heterogeneous transformation mechanism was assumed to be the same for day and night. Therefore, the daytime heterogeneous productivity ($P_{het} = C_{HONO} \times [NO_2]$) was calculated with the nighttime mean values of C_{HONO} in different periods. $L_{OH+HONO}$ is the rate of the reaction between OH and HONO (R3). The calculation formulas of P_{OH+NO} and $L_{OH+HONO}$ have been provided in **Section 3.2.1**. Upon sunlight irradiation, ·OH and NO were formed as R1. L_{photo} represents the photolysis loss rate of HONO ($L_{photo} = J_{HONO} \times [HONO]$). The photolysis frequency and ·OH concentration could not be directly measured in this study. Therefore, the tropospheric ultraviolet and visible (TUV) transfer model of the National Center for Atmospheric Research (http://cprm.acom.ucar.edu/Models/TUV/

477 Interactive_TUV/) (Hou et al., 2016) was used to calculate the J_{HONO} value.

478 The J_{HONO} values obtained this way were assumed in clear sky days without clouds. O_3

479 column and the surface albedo. O_3 column density measured by the Ozone Monitoring

480 Instrument (OMI, data available at https://ozonewatch.gsfc.nasa.gov/data/omi/Y2019/).

481 The O_3 column density ranges from 292 to 306 DU during the entire period. The

482 experimental site being situated in an urban region, the surface albedo is considered as

483 0.13 (Sailor, 1995). The ground elevation and the measurement altitude are 168 and

484 188 m respectively. The concentration of OH radicals was calculated with the formulas

485 of NO_2, O_3, and J_{O^1D} in the supplement (Rohrer and Berresheim, 2006). Aerosol

486 effects were considered by using aerosol optical thickness (AOD), single

487 scattering albedo (SSA), and Angstrom exponent as inputs in the TUV

488 model. Typical AOD, SSA, and Angstrom exponent values of 1.32, 0.9, and

489 1.3, respectively, were adopted for the PD and SPD periods. In the CD

490 period, the respective values were 0.66, 0.89, and 1.07 (Che et al., 2015;

491 Cui et al., 2018; Hou et al., 2016). We wanted to study that under the same

492 output conditions from the TUV model in the PD and SPD periods, the

493 impact of different pollution levels changed on the daytime budget. Hence,

494 the average profiles of J_{HONO} and J_{O^1D} concentrations in the CD, PD, and

495 SPD periods are shown in **Fig. 9**. The mean values of J_{HONO} and ·OH

496 concentration at noon in the CD, PD, and SPD periods were 5.93×10^{-4},

497 3.79×10^{-4}, and 3.79×10^{-4} molecule cm^{-3} and 4.10×10^6, 2.93×10^6, and

498 3.76×10^6 molecule cm^{-3}, respectively. The results of the calculated OH radicals

499 ranged from $(0.58-11.49) \times 10^6$ molecule cm^{-3}, and the mean value was 3.57×10^6

500 molecule cm^{-3} at noon in Zhengzhou.

501   Each production and loss rate of daytime HONO during CD, PD, and

502 SPD periods is illustrated in **Fig. 9** together with dHONO/dt. $P_{unknown}$ was at

503 a high level before midday. $P_{unknown}$ approached 0 ppbv h^{-1} after midday. In

504 the CD, PD, and SPD periods, the mean values of $P_{unknown}$ were 0.26, 0.40,

and 1.83 ppbv h^{-1}, respectively; the mean values of P_{OH+NO} were 1.14, 2.07, and 4.03 ppbv h^{-1}, respectively; the mean values of P_{emi} were 0.17, 0.30, and 0.43 ppbv h^{-1}, respectively; and the mean values of P_{het} were 0.14, 0.18, and 0.55 ppbv h^{-1}, respectively. The midday time $P_{unknown}$ (1.83 ppbv h^{-1}) calculated in Zhengzhou during the winter haze pollution period was close to the result obtained from Beijing's urban area (Hou et al., 2016) (1.85 ppbv h^{-1}). The $P_{unknown}$ contribution to daytime HONO sources in CD, PD, and SPD periods accounted for 15, 14, and 28% of the HONO production rate ($P_{unknown} + P_{OH+NO} + P_{emi} + P_{het}$), respectively. Previous studies (Spataro et al., 2013; Yang et al., 2014) have shown that meteorological conditions, such as solar radiation and WS, can affect unknown sources. The low $P_{unknown}$ contribution of daytime HONO concentration may be related to the low solar radiation and low wind speed during severe pollution. The concentration of NO has a great influence on P_{OH+NO}, so the homogeneous reaction is still an important pathway of HONO production during the daytime. In addition to the photolysis of HONO and the homogeneous reaction of HONO and OH, one or more important sinks might exist to control the variation between the sources and sinks of the daytime HONO during complex contamination. However, further research is needed to analyze the unknown sources of daytime HONO.

4. Conclusions

Ambient HONO measurement using AIM with other atmospheric pollutants and meteorological parameters was conducted in the CPER. The HONO concentrations during the entire measurement varied from 0.2 to 14.8 ppbv, with an average of 2.5 ppbv. The HONO concentrations in the CD, PD, and SPD periods were 1.1, 2.3, and 3.7 ppbv, respectively, and the HONO/NO_2 ratios were 4.7, 7.1, and 9.4%, respectively. HONO concentration was a combined action of direct emission and heterogeneous reaction, and the contributions of the two were higher than that of homogeneous reaction in the first half of the night. However, the proportion of homogenization gradually increased in the second half of the night due to the steady increase in NO

concentration. The hourly level of other HONO abatement pathways aside from OH +

HONO should be at least 0.22 ppbv h^{-1} in the SPD period. The sum of the frequency

distributions of the HONO$_{emission}$/HONO ratio (less than 20%) was approximately 77%,

indicating that the direct emission of HONO was not the main source of the observed

HONO level at night. The mean values of HONO$_{emission}$/HONO in the CD, PD, and SPD

periods were 17, 16, and 16%, respectively. This phenomenon means that the policy of

restricting motor vehicles published by the local government in January 2019 had a

good effect on decreasing HONO emissions. In addition, when RH increased at the

middle level, the heterogeneous HONO production increased, but it decreased when

RH increased further due to the effect of surface water. The contribution of the three

sources varied with different pollution levels. The mean values of C$_{HONO}$ in the

CD, PD, and SPD periods were 0.72×10^{-2}, 0.64×10^{-2}, and 1.54×10^{-2} h^{-1},

respectively. At nighttime in the SPD period, the heterogeneous conversion of NO$_2$

appeared to be unimportant. Furthermore, the net production generated by

homogeneous reaction may be the leading factor for the increase in HONO under high-

NO$_X$ conditions (i.e., the concentration of NO was relatively higher than that of NO$_2$)

at nighttime. The mean value of P_{OH+NO}^{net} in the CD, PD, and SPD periods were 0.13,

0.26, and 0.56 ppbv h^{-1}, respectively. Daytime HONO budget analysis showed that the

mean values of P$_{unknown}$ in the CD, PD, and SPD periods were 0.26, 0.40, and 1.83 ppbv

h^{-1}, respectively. Although the values of P$_{OH+NO}$ had high uncertainty because of the

variation of NO concentrations, P$_{OH+NO}$ contributed the most to HONO production

during the daytime. After the analysis, C$_{HONO}$, P_{OH+NO}^{net}, and P$_{unknown}$ in the SPD period

were larger than those in the other periods, indicating that HONO participated in many

reactions.

Acknowledgments

561   (162300410255).

Reference

Acker, K., Möller, D., Auel, R., Wieprecht, W., and Kalaß, D.: Concentrations of
nitrous acid, nitric acid, nitrite and nitrate in the gas and aerosol phase at a site in
the emission zone during ESCOMPTE 2001 experiment, Atmos. Res., 74, 507-524,
https://doi.org/10.1016/j.atmosres.2004.04.009, 2005.

Alicke, B., Platt, U., and Stutz, J.: Impact of nitrous acid photolysis on the total
hydroxyl radical budget during the Limitation of Oxidant Production/Pianura
Padana Produzione di Ozono study in Milan, J. Geophys. Res.,
https://doi.org/10.1029/2000jd000075, 2002.

Alicke, B.: OH formation by HONO photolysis during the BERLIOZ experiment, J.
Geophys. Res., 108, https://doi.org/10.1029/2001jd000579, 2003.

Ammann, M., Kalberer, M., Jost, D. T., Tobler, L., Rössler, E., Piguet, D., Gäggeler,
H. W., and Baltensperger, U.: Heterogeneous production of nitrous acid on soot in
polluted air masses, Nature, 395, 157-160, https://doi.org/10.1038/25965, 1998.

An, J., Li, Y., Chen, Y., Li, J., Qu, Y., and Tang, Y.: Enhancements of major aerosol
components due to additional HONO sources in the North China Plain and
implications for visibility and haze, Adv. Atoms. Sci., 30, 57-66,
https://doi.org/10.1007/s00376-012-2016-9, 2012.

Atkinson, R., Baulch, D. L., Cox, R. A., Crowley, J. N., Hampson, R. F., Hynes, R.
G., Jenkin, M. E., Rossi, M. J., and Troe, J.: Evaluated kinetic and photochemical
data for atmospheric chemistry: Volume I - gas phase reactions of O_x, HO_x, NO_x
and SO_x species, Atmos. Chem. Phys., 4, 1461-1738, https://doi.org/10.5194/acp-4-
1461-2004, 2004.

Che, H., Xia, X., Zhu, J., Wang, H., Wang, Y., Sun, J., Zhang, X., and Shi, G.: Aerosol
optical properties under the condition of heavy haze over an urban site of Beijing,
China, Environ. Sci. Pollut. Res., 22, 1043-1053, https://doi.org/10.1007/s11356-
014-3415-5, 2015.

589   Cui, L., Li, R., Zhang, Y., Meng, Y., Fu, H., and Chen, J.: An observational study of

590   nitrous acid (HONO) in Shanghai, China: The aerosol impact on HONO formation

591   during the haze episodes, Sci. Total Environ., 630, 1057-1070,

592   https://doi.org/10.1016/j.scitotenv.2018.02.063, 2018.

593   Czader, B. H., Rappenglück, B., Percell, P., Byun, D. W., Ngan, F., and Kim, S.:

594   Modeling nitrous acid and its impact on ozone and hydroxyl radical during the

595   Texas Air Quality Study 2006, Atmos. Chem. Phys., 12, 6939-6951,

596   https://doi.org/10.5194/acp-12-6939-2012, 2012.

597   Duan, J., Qin, M., Ouyang, B., Fang, W., Li, X., Lu, K., Tang, K., Liang, S., Meng, F.,

598   Hu, Z., Xie, P., Liu, W., and Häsler, R.: Development of an incoherent broadband

599   cavity-enhanced absorption spectrometer for in situ measurements of HONO and

600   NO_2, Atmos. Meas. Tech., 11, 4531-4543, https://doi.org/10.5194/amt-11-4531-

601   2018, 2018.

602   Elshorbany, Y. F., Steil, B., Brühl, C., and Lelieveld, J.: Impact of HONO on global

603   atmospheric chemistry calculated with an empirical parameterization in the EMAC

604   model, Atmos. Chem. Phys., 12, 9977-10000, https://doi.org/10.5194/acp-12-9977-

605   2012, 2012.

606   Elshorbany, Y. F., Crutzen, P. J., Steil, B., Pozzer, A., Tost, H., and Lelieveld, J.:

607   Global and regional impacts of HONO on the chemical composition of clouds and

608   aerosols, Atmos. Chem. Phys., 14, 1167-1184, https://doi.org/10.5194/acp-14-1167-

609   2014, 2014.

610   Finlayson-Pitts, B. J., Wingen, L. M., Sumner, A. L., Syomin, D., and Ramazan, K.

611   A.: The heterogeneous hydrolysis of NO2 in laboratory systems and in outdoor and

612   indoor atmospheres: An integrated mechanism, PCCP, 5, 223-242,

613   https://doi.org/10.1039/b208564j, 2003.

614   Grassian, V. H.: Heterogeneous uptake and reaction of nitrogen oxides and volatile

615   organic compounds on the surface of atmospheric particles including oxides,

616   carbonates, soot and mineral dust: Implications for the chemical balance of the

617   troposphere, Int. Rev. Phys. Chem., 20, 467-548,

618   https://doi.org/10.1080/01442350110051968, 2001.

619   Hao, N., Zhou, B., Chen, D., and Chen, L.: Observations of nitrous acid and its

620   relative humidity dependence in Shanghai, J. Environ. Sci.-China, 18, 910-915,

621   https://doi.org/10.1016/s1001-0742(06)60013-2, 2006.

622   Harrison, R. M., Peak, J. D., and Collins, G. M.: Tropospheric cycle of nitrous acid, J.

623   Geophys. Res., 101, 14429-14439, https://doi.org/10.1029/96jd00341, 1996.

624   Harrison, R. M., and Collins, G. M.: Measurements of Reaction Coefficients of NO2

625   and HONO on Aerosol Particles, J. Atmos. Chem., 30, 397-406,

626   https://doi.org/10.1023/A:1006094304069, 1998.

627   Heland, J., Kleffmann, J., Kurtenbach, R., and Wiesen, P.: A new instrument to

628   measure gaseous nitrous acid (HONO) in the atmosphere, Environ. Sci. Technol.,

629   35, 3207-3212, https://doi.org/10.1021/es000303t, 2001.

630   Hendrick, F., Müller, J. F., Clémer, K., Wang, P., De Mazière, M., Fayt, C., Gielen, C.,

631   Hermans, C., Ma, J. Z., Pinardi, G., Stavrakou, T., Vlemmix, T., and Van

632   Roozendael, M.: Four years of ground-based MAX-DOAS observations of HONO

633   and NO_2 in the Beijing area, Atmos. Chem. Phys., 14, 765-781,

634   https://doi.org/10.5194/acp-14-765-2014, 2014.

635   Hirokawa, J., Kato, T., and Mafuné, F.: In Situ Measurements of Atmospheric Nitrous

636   Acid by Chemical Ionization Mass Spectrometry Using Chloride Ion Transfer

637   Reactions, Anal. Chem., 81, 8380-8386, https://doi.org/10.1021/ac901117b, 2009.

638   Hou, S., Tong, S., Ge, M., and An, J.: Comparison of atmospheric nitrous acid during

639   severe haze and clean periods in Beijing, China, Atmos. Environ., 124, 199-206,

640   https://doi.org/10.1016/j.atmosenv.2015.06.023, 2016.

641   Huang, R. J., Yang, L., Cao, J., Wang, Q., Tie, X., Ho, K. F., Shen, Z., Zhang, R., Li,

642   G., Zhu, C., Zhang, N., Dai, W., Zhou, J., Liu, S., Chen, Y., Chen, J., and O'Dowd,

643   C. D.: Concentration and sources of atmospheric nitrous acid (HONO) at an urban

644 site in Western China, Sci. Total Environ., 593-594, 165-172,

645 https://doi.org/10.1016/j.scitotenv.2017.02.166, 2017.

646 Jiang, N., Dong, Z., Xu, Y., Yu, F., Yin, S., Zhang, R., and Tang, X.: Characterization

647 of PM_{10} and $PM_{2.5}$ Source Profiles of Fugitive Dust in Zhengzhou, China, Aerosol

648 Air Qual. Res., 18, 314-329, https://doi.org/10.4209/aaqr.2017.04.0132, 2018a.

649 Jiang, N., Wang, K., Yu, X., Su, F., Yin, S., Li, Q., and Zhang, R.: Chemical

650 characteristics and source apportionment by two receptor models of size-segregated

651 aerosols in an emerging megacity in China, Aerosol Air Qual. Res., 18, 1375–1390,

652 https://doi.org/10.4209/aaqr.2017.10.0413, 2018b.

653 Jiang, N., Liu, X., Wang, S., Yu, X., Yin, S., Duan, S., Shenbo, W., Zhang, R., and Li,

654 S.: Pollution characterization, source identification, and health risks of

655 atmospheric-particle-bound heavy metals in PM_{10} and $PM_{2.5}$ at multiple sites in an

656 emerging megacity in the Central Region of China, Aerosol Air Qual. Res., 19,

657 247-271, https://doi.org/10.4209/aaqr.2018.07.0275, 2019.

658 Kim, D.-R., Lee, J.-B., Keun Song, C., Kim, S.-Y., Ma, Y.-l., Lee, K.-M., Cha, J.-S.,

659 and Lee, S.-D.: Temporal and spatial distribution of tropospheric NO_2 over

660 Northeast Asia using OMI data during the years 2005–2010, Atmos. Pollut. Res., 6,

661 768-776, https://doi.org/10.5094/apr.2015.085, 2015.

662 Kleffmann, J., Becker, K. H., Lackhoff, M., and Wiesen, P.: Heterogeneous

663 conversion of NO2 on carbonaceous surfaces, PCCP, 1, 5443-5450,

664 https://doi.org/10.1039/a905545b, 1999.

665 Kurtenbach, R., Becker, K. H., Gomes, J. A. G., Kleffmann, J., Lorzer, J. C., Spittler,

666 M., Wiesen, P., Ackermann, R., Geyer, A., and Platt, U.: Investigations of

667 emissions and heterogeneous formation of HONO in a road traffic tunnel, Atmos.

668 Environ., 35, 3385-3394, https://doi.org/10.1016/s1352-2310(01)00138-8, 2001.

669 Lelieveld, J., Gromov, S., Pozzer, A., and Taraborrelli, D.: Global tropospheric

670 hydroxyl distribution, budget and reactivity, Atmos. Chem. Phys., 16, 12477-

671 12493, https://doi.org/10.5194/acp-16-12477-2016, 2016.

672   Li, Q., Jiang, N., Yu, X., Dong, Z., Duan, S., Zhang, L., and Zhang, R.: Sources and

673   spatial distribution of PM2.5-bound polycyclic aromatic hydrocarbons in

674   Zhengzhou in 2016, Atmos. Res., 216, 65–75,

675   https://doi.org/10.1016/j.atmosres.2018.09.011, 2019.

676   Li, X., Brauers, T., Häseler, R., Bohn, B., Fuchs, H., Hofzumahaus, A., Holland, F.,

677   Lou, S., Lu, K. D., Rohrer, F., Hu, M., Zeng, L. M., Zhang, Y. H., Garland, R. M.,

678   Su, H., Nowak, A., Wiedensohler, A., Takegawa, N., Shao, M., and Wahner, A.:

679   Exploring the atmospheric chemistry of nitrous acid (HONO) at a rural site in

680   Southern China, Atmos. Chem. Phys., 12, 1497-1513, https://doi.org/10.5194/acp-

681   12-1497-2012, 2012.

682   Liu, F., Beirle, S., Zhang, Q., van der, A. R., Zheng, B., Tong, D., and He, K.: NOx

683   emission trends over Chinese cities estimated from OMI observations during 2005

684   to 2015, Atmos Chem Phys, 17, 9261-9275, https://doi.org/10.5194/acp-17-9261-

685   2017, 2017.

686   Liu, X., Jiang, N., Yu, X., Zhang, R., Li, S., Li, Q., and Kang, P.: Chemical

687   characteristics, sources apportionment, and risk assessment of PM2.5 in different

688   functional areas of an emerging megacity in China, Aerosol Air Qual. Res., 19,

689   2222-2238, https://doi.org/10.4209/aaqr.2019.02.0076, 2019.

690   Liu, Z., Wang, Y., Costabile, F., Amoroso, A., Zhao, C., Huey, L. G., Stickel, R., Liao,

691   J., and Zhu, T.: Evidence of aerosols as a media for rapid daytime HONO

692   production over China, Environ. Sci. Technol., 48, 14386-14391,

693   https://doi.org/10.1021/es504163z, 2014.

694   Lu, X., Wang, Y., Li, J., Shen, L., and Fung, J. C. H.: Evidence of heterogeneous

695   HONO formation from aerosols and the regional photochemical impact of this

696   HONO source, Environ. Res. Lett., 13, https://doi.org/10.1088/1748-9326/aae492,

697   2018.

698   Markovic, M. Z., VandenBoer, T. C., and Murphy, J. G.: Characterization and

699   optimization of an online system for the simultaneous measurement of atmospheric

700   water-soluble constituents in the gas and particle phases, J. Environ. Monit., 14,

701   1872-1884, https://doi.org/10.1039/c2em00004k, 2012.

702 Michoud, V., Colomb, A., Borbon, A., Miet, K., Beekmann, M., Camredon, M.,

703   Aumont, B., Perrier, S., Zapf, P., Siour, G., Ait-Helal, W., Afif, C., Kukui, A.,

704   Furger, M., Dupont, J. C., Haeffelin, M., and Doussin, J. F.: Study of the unknown

705   HONO daytime source at a European suburban site during the MEGAPOLI

706   summer and winter field campaigns, Atmos. Chem. Phys., 14, 2805-2822,

707   https://doi.org/10.5194/acp-14-2805-2014, 2014.

708 Min, K. E., Washenfelder, R. A., Dubé, W. P., Langford, A. O., Edwards, P. M.,

709   Zarzana, K. J., Stutz, J., Lu, K., Rohrer, F., Zhang, Y., and Brown, S. S.: A

710   broadband cavity enhanced absorption spectrometer for aircraft measurements of

711   glyoxal, methylglyoxal, nitrous acid, nitrogen dioxide, and water vapor, Atmos.

712   Meas. Tech., 9, 423-440, https://doi.org/10.5194/amt-9-423-2016, 2016.

713 Pinto, J. P., Dibb, J., Lee, B. H., Rappenglück, B., Wood, E. C., Levy, M., Zhang, R.

714   Y., Lefer, B., Ren, X. R., Stutz, J., Tsai, C., Ackermann, L., Golovko, J., Herndon,

715   S. C., Oakes, M., Meng, Q. Y., Munger, J. W., Zahniser, M., and Zheng, J.:

716   Intercomparison of field measurements of nitrous acid (HONO) during the SHARP

717   campaign, J. Geophys. Res.-Atmos., 119, 5583-5601,

718   https://doi.org/10.1002/2013jd020287, 2014.

719 Qin, M., Xie, P., Su, H., Gu, J., Peng, F., Li, S., Zeng, L., Liu, J., Liu, W., and Zhang,

720   Y.: An observational study of the HONO–NO_2 coupling at an urban site in

721   Guangzhou City, South China, Atmos. Environ., 43, 5731-5742,

722   https://doi.org/10.1016/j.atmosenv.2009.08.017, 2009.

723 Rappenglück, B., Lubertino, G., Alvarez, S., Golovko, J., Czader, B., and Ackermann,

724   L.: Radical precursors and related species from traffic as observed and modeled at

725   an urban highway junction, J. Air Waste Manage. Assoc., 63, 1270-1286,

726   https://doi.org/10.1080/10962247.2013.822438, 2013.

727   Roberts, J. M., Veres, P., Warneke, C., Neuman, J. A., Washenfelder, R. A., Brown, S.

728   S., Baasandorj, M., Burkholder, J. B., Burling, I. R., Johnson, T. J., Yokelson, R. J.,

729   and de Gouw, J.: Measurement of HONO, HNCO, and other inorganic acids by

730   negative-ion proton-transfer chemical-ionization mass spectrometry (NI-PT-

731   CIMS): application to biomass burning emissions, Atmos. Meas. Tech., 3, 981-990,

732   https://doi.org/10.5194/amt-3-981-2010, 2010.

733   Rohrer, F., and Berresheim, H.: Strong correlation between levels of tropospheric

734   hydroxyl radicals and solar ultraviolet radiation, Nature, 442, 184-187,

735   https://doi.org/10.1038/nature04924, 2006.

736   Sailor, D. J.: Simulated Urban Climate Response to Modifications in Surface Albedo

737   and Vegetative Cover, J. Appl. Meteorol., 34, 1694-1704,

738   https://doi.org/10.1175/1520-0450-34.7.1694, 1995.

739   Sander, S., Friedl, R., Golden, D., Kurylo, M., Huie, R., Orkin, V., Moortgat, G.,

740   Ravishankara, A. R., Kolb, C., Molina, M., and Finlayson-Pitts, B.: Chemical

741   Kinetics and Photochemical Data for Use in Atmospheric Studies; JPL Publication

742   02-25, 2003.

743   Shen, L. J., and Zhang, Z. F.: Heterogeneous reactions of NO_2 on the surface of black

744   carbon, Prog. Chem., 25, 28-35, 2013.

745   Sörgel, M., Regelin, E., Bozem, H., Diesch, J. M., Drewnick, F., Fischer, H., Harder,

746   H., Held, A., Hosaynali-Beygi, Z., Martinez, M., and Zetzsch, C.: Quantification of

747   the unknown HONO daytime source and its relation to NO_2, Atmos. Chem. Phys.,

748   11, 10433-10447, https://doi.org/10.5194/acp-11-10433-2011, 2011.

749   Spataro, F., Ianniello, A., Esposito, G., Allegrini, I., Zhu, T., and Hu, M.: Occurrence

750   of atmospheric nitrous acid in the urban area of Beijing (China), Sci. Total

751   Environ., 447, 210-224, https://doi.org/10.1016/j.scitotenv.2012.12.065, 2013.

752   Stutz, J.: Nitrous acid formation in the urban atmosphere: Gradient measurements of

753   NO_2 and HONO over grass in Milan, Italy, J. Geophys. Res., 107,

754   https://doi.org/10.1029/2001jd000390, 2002.

755   Stutz, J., Alicke, B., Ackermann, R., Geyer, A., Wang, S., White, A. B., Williams, E.

756   J., Spicer, C. W., and Fast, J. D.: Relative humidity dependence of HONO

757   chemistry in urban areas, J. Geophys. Res., 109, 03307-03319,

758   https://doi.org/10.1029/2003jd004135, 2004.

759   Su, H., Cheng, Y. F., Cheng, P., Zhang, Y. H., Dong, S., Zeng, L. M., Wang, X.,

760   Slanina, J., Shao, M., and Wiedensohler, A.: Observation of nighttime nitrous acid

761   (HONO) formation at a non-urban site during PRIDE-PRD2004 in China, Atmos.

762   Environ., 42, 6219-6232, https://doi.org/10.1016/j.atmosenv.2008.04.006, 2008a.

763   Su, H., Cheng, Y. F., Shao, M., Gao, D. F., Yu, Z. Y., Zeng, L. M., Slanina, J., Zhang,

764   Y. H., and Wiedensohler, A.: Nitrous acid (HONO) and its daytime sources at a

765   rural site during the 2004 PRIDE-PRD experiment in China, J. Geophys. Res., 113,

766   D14312-14321, https://doi.org/10.1029/2007jd009060, 2008b.

767   Tan, Z., Rohrer, F., Lu, K., Ma, X., Bohn, B., Broch, S., Dong, H., Fuchs, H.,

768   Gkatzelis, G. I., Hofzumahaus, A., Holland, F., Li, X., Liu, Y., Liu, Y., Novelli, A.,

769   Shao, M., Wang, H., Wu, Y., Zeng, L., Hu, M., Kiendler-Scharr, A., Wahner, A.,

770   and Zhang, Y.: Wintertime photochemistry in Beijing: observations of RO_x radical

771   concentrations in the North China Plain during the BEST-ONE campaign, Atmos.

772   Chem. Phys., 18, 12391-12411, https://doi.org/10.5194/acp-18-12391-2018, 2018.

773   Tian, Y., Xue, Q., Xiao, Z., Chen, K., and Feng, Y.: PMF-GAS Methods to Estimate

774   Contributions of Sources and Oxygen for $PM_{2.5}$, Based on Highly Time-Resolved

775       $PM_{2.5}$ Species and Gas Data, Aerosol Air Qual. Res., 18, 2956-2966,

776   https://doi.org/10.4209/aaqr.2018.07.0244, 2018.

777   Tong, S., Hou, S., Zhang, Y., Chu, B., Liu, Y., He, H., Zhao, P., and Ge, M.:

778   Comparisons of measured nitrous acid (HONO) concentrations in a pollution

779   period at urban and suburban Beijing, in autumn of 2014, Sci. China Chem., 58,

780   1393-1402, https://doi.org/10.1007/s11426-015-5454-2, 2015.

781   Tong, S., Hou, S., Zhang, Y., Chu, B., Liu, Y., He, H., Zhao, P., and Ge, M.: Exploring

782   the nitrous acid (HONO) formation mechanism in winter Beijing: direct emissions

783 and heterogeneous production in urban and suburban areas, Faraday Discuss., 189,

784 213-230, https://doi.org/10.1039/c5fd00163c, 2016.

785 VandenBoer, T. C., Markovic, M. Z., Sanders, J. E., Ren, X., Pusede, S. E., Browne,

786 E. C., Cohen, R. C., Zhang, L., Thomas, J., Brune, W. H., and Murphy, J. G.:

787 Evidence for a nitrous acid (HONO) reservoir at the ground surface in Bakersfield,

788 CA, during CalNex 2010, J. Geophys. Res.-Atmos., 119, 9093-9106,

789 https://doi.org/10.1002/2013jd020971, 2014.

790 Vogel, B., Vogel, H., Kleffmann, J., and Kurtenbach, R.: Measured and simulated

791 vertical profiles of nitrous acid—Part II. Model simulations and indications for a

792 photolytic source, Atmos. Environ., 37, 2957-2966, https://doi.org/10.1016/s1352-

793 2310(03)00243-7, 2003.

794 Wang, S., Zhou, R., Zhao, H., Wang, Z., Chen, L., and Zhou, B.: Long-term

795 observation of atmospheric nitrous acid (HONO) and its implication to local NO_2

796 levels in Shanghai, China, Atmos. Environ., 77, 718-724,

797 https://doi.org/10.1016/j.atmosenv.2013.05.071, 2013.

798 Wang, S., Yin, S., Zhang, R., Yang, L., Zhao, Q., Zhang, L., Yan, Q., Jiang, N., and

799 Tang, X.: Insight into the formation of secondary inorganic aerosol based on high-

800 time-resolution data during haze episodes and snowfall periods in Zhengzhou,

801 China, Sci. Total Environ., 660, 47-56,

802 https://doi.org/10.1016/j.scitotenv.2018.12.465, 2019.

803 Winer, A. M., and Biermann, H. W.: Long pathlength differential optical absorption

804 spectroscopy (DOAS) measurements of gaseous HONO, NO_2 and HCNO in the

805 California South Coast Air Basin, Res. Chem. Intermed., 20, 423-445,

806 https://doi.org/10.1163/156856794X00405, 1994.

807 Wojtal, P., Halla, J. D., and McLaren, R.: Pseudo steady states of HONO measured in

808 the nocturnal marine boundary layer: a conceptual model for HONO formation on

809 aqueous surfaces, Atmos. Chem. Phys., 11, 3243-3261, https://doi.org/10.5194/acp-

810 11-3243-2011, 2011.

811   Xu, Z., Wang, T., Wu, J., Xue, L., Chan, J., Zha, Q., Zhou, S., Louie, P. K. K., and

812   Luk, C. W. Y.: Nitrous acid (HONO) in a polluted subtropical atmosphere:

813   Seasonal variability, direct vehicle emissions and heterogeneous production at

814   ground surface, Atmos. Environ., 106, 100-109,

815   https://doi.org/10.1016/j.atmosenv.2015.01.061, 2015.

816   Yang, Q., Su, H., Li, X., Cheng, Y., Lu, K., Cheng, P., Gu, J., Guo, S., Hu, M., Zeng,

817   L., Zhu, T., and Zhang, Y.: Daytime HONO formation in the suburban area of the

818   megacity Beijing, China, Sci. China Chem., 57, 1032-1042,

819   https://doi.org/10.1007/s11426-013-5044-0, 2014.

820   Zhang, B., and Tao, F.-M.: Direct homogeneous nucleation of NO_2, H_2O, and NH_3

821   for the production of ammonium nitrate particles and HONO gas, Chem. Phys.

822   Lett., 489, 143-147, https://doi.org/10.1016/j.cplett.2010.02.059, 2010.

823   Zhang, W., Tong, S., Ge, M., An, J., Shi, Z., Hou, S., Xia, K., Qu, Y., Zhang, H., Chu,

824   B., Sun, Y., and He, H.: Variations and sources of nitrous acid (HONO) during a

825   severe pollution episode in Beijing in winter 2016, Sci. Total Environ., 648, 253-

826   262, https://doi.org/10.1016/j.scitotenv.2018.08.133, 2019.

827

Figure Captions:

Fig. 1. Temporal trends of hourly average T, RH, WD, WS, and $PM_{2.5}$ during the measurement. (The shaded areas: white for the CD period; gray for the PD period; red for the SPD period.)

Fig. 2. Temporal variations of hourly average HONO, NO, NO_2, O_3, and CO during the measurement. (The shaded areas: white for the CD period; gray for the PD period; red for the SPD period.)

Fig. 3. Diurnal variations of HONO during the measurement.

Fig. 4. Diurnal variations of HONO, NO, NO_2, O_3, $HONO/NO_2$, and $HONO/NO_X$. The blue points and lines represented the CD period; the black points and lines represented the PD period; the red points and lines represented the SPD period.

Fig. 5. Nocturnal variations of P_{OH+NO}^{net}, HONO and NO during CD, PD and SPD periods.

Fig. 6. Percentage distribution of the nighttime $HONO_{emission}/HONO$. (The dotted line represents the average of $HONO_{emission}/HONO$.)
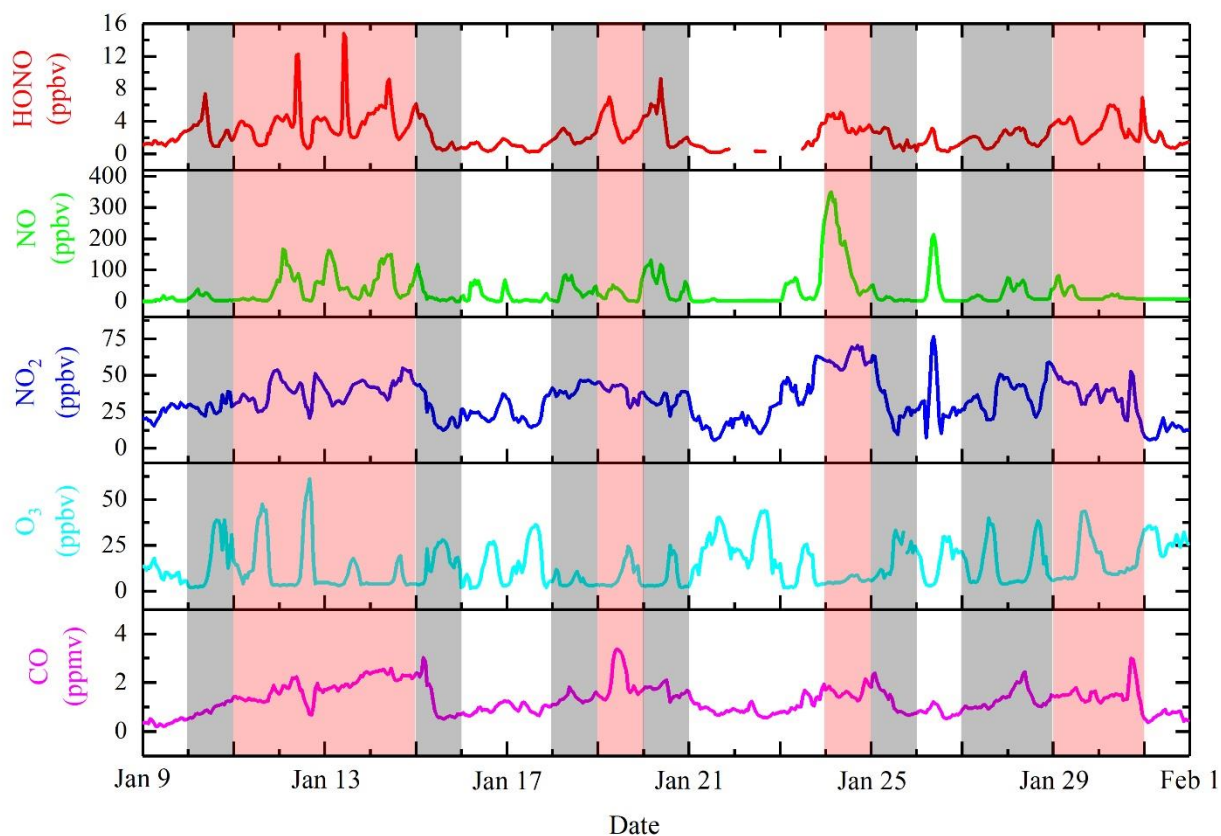
Fig. 7. Nighttime correlation studies between $PM_{2.5}$ and $HONO/NO_2$, $PM_{2.5}$ and HONO, CO and HONO, RH and $HONO/NO_2$ during the entire measurement period, CD, PD, and SPD periods. The blue represented the full measurement period; the light blue represented CD period; the black represented PD period; the red represented SPD period.

Fig. 8. Nocturnal variations of $HONO_{correct}$, NO_2, and $HONO_{correct}/NO_2$ in CD, PD and SPD periods.
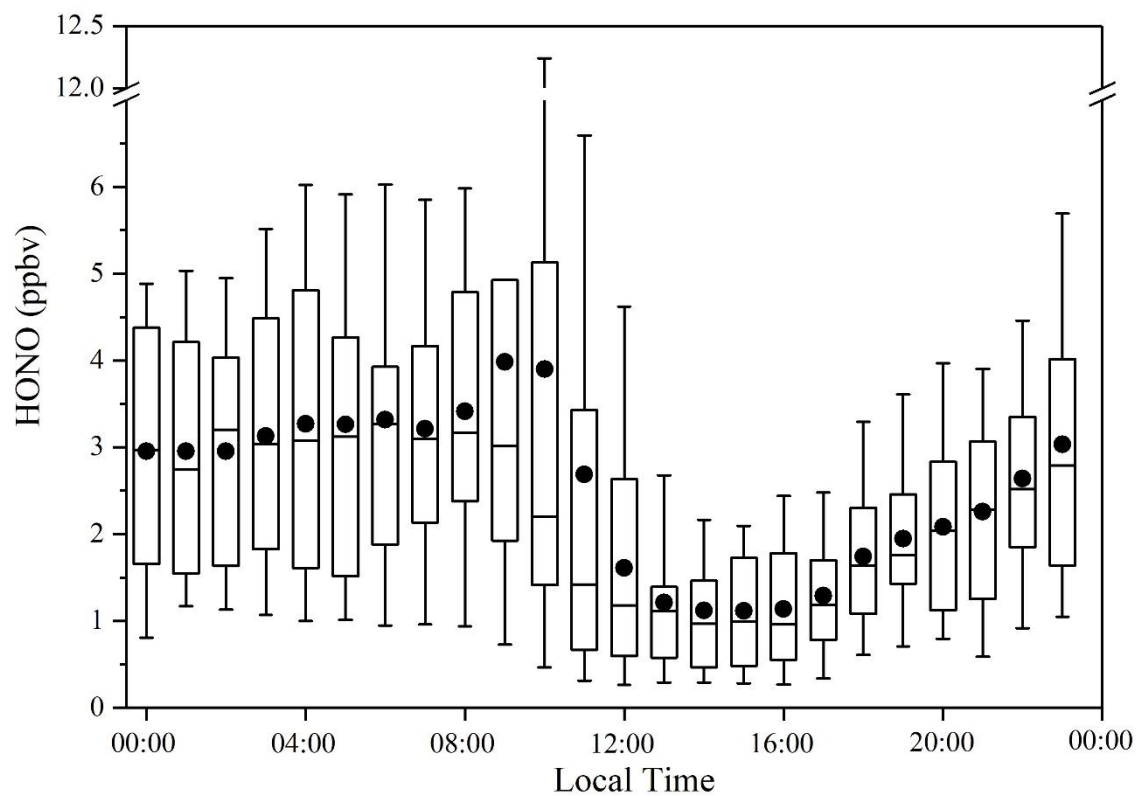
Fig. 9. The average profiles of J_{HONO} and $J_O{}^1{}_D$ concentrations during the daytime, and production and loss rate of the daytime HONO in CD, PD and SPD periods.
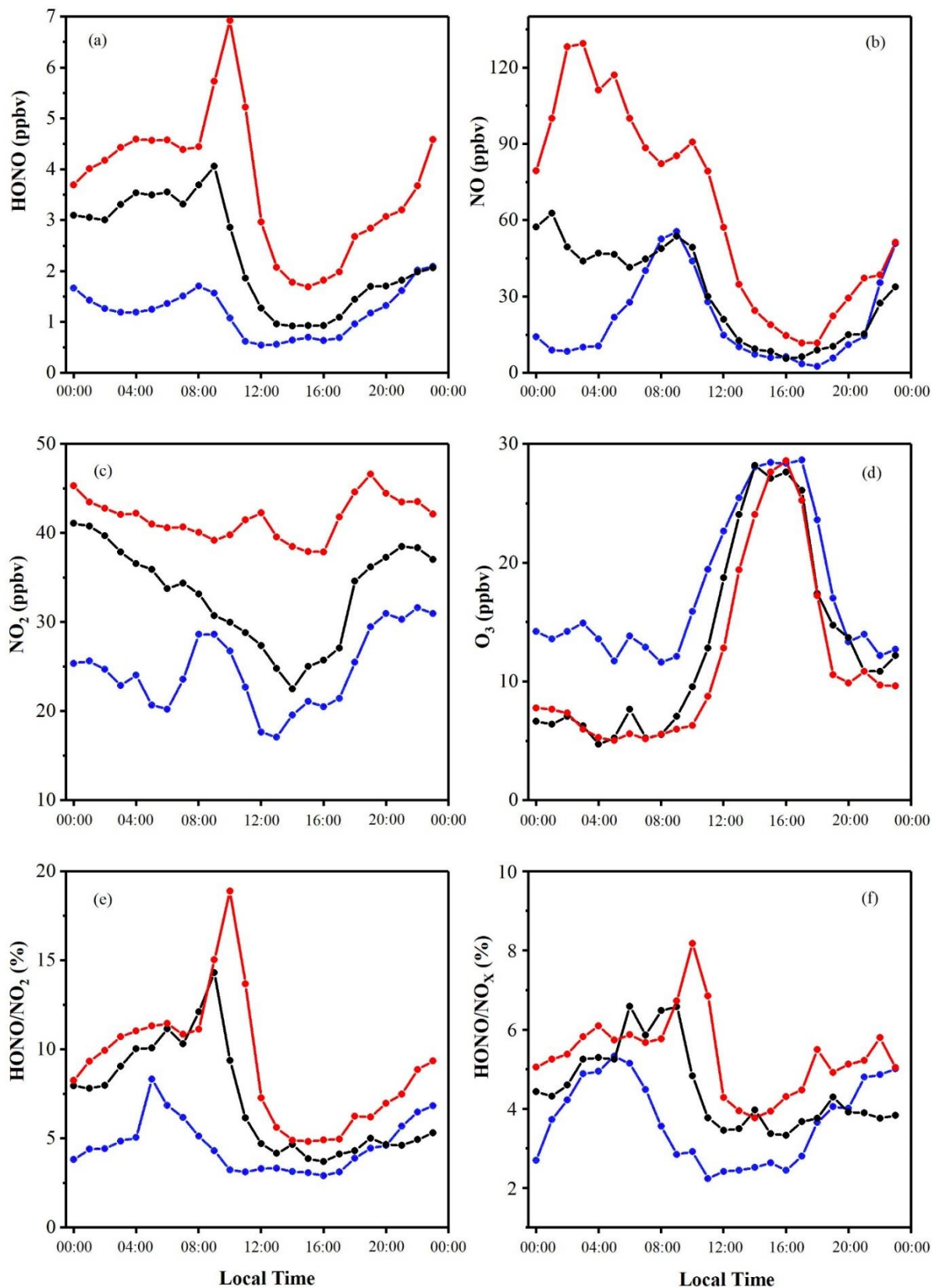
Fig. 1. Temporal trends of hourly average T, RH, WD, WS, and PM$_{2.5}$ during the measurement. (The shaded areas: white for the CD period; gray for the PD period; red for the SPD period.)
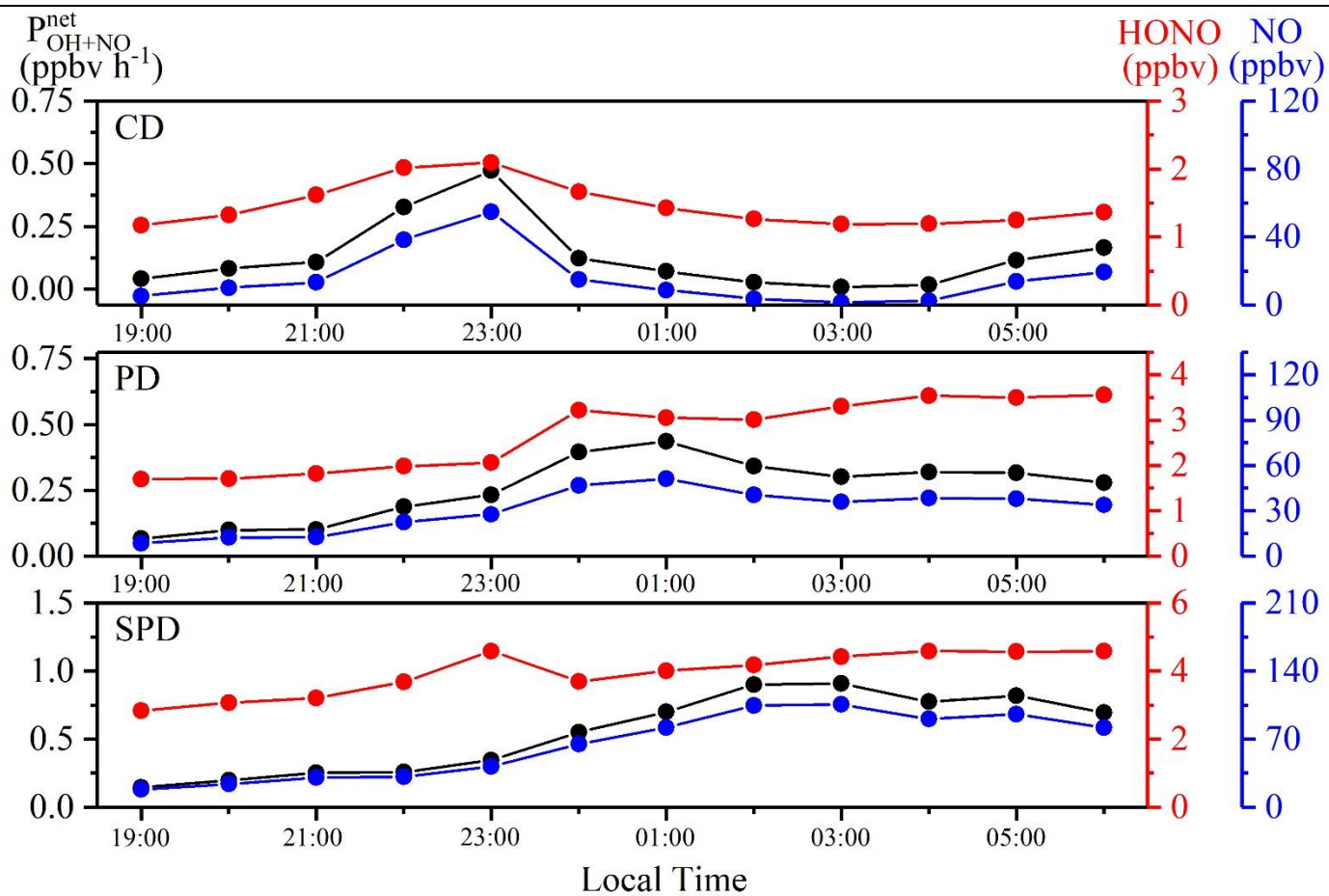
Fig. 2. Temporal variations of hourly average HONO, NO, NO$_2$, O$_3$, and CO during the measurement. (The shaded areas: white for the CD period; gray for the PD period; red for the SPD period.)
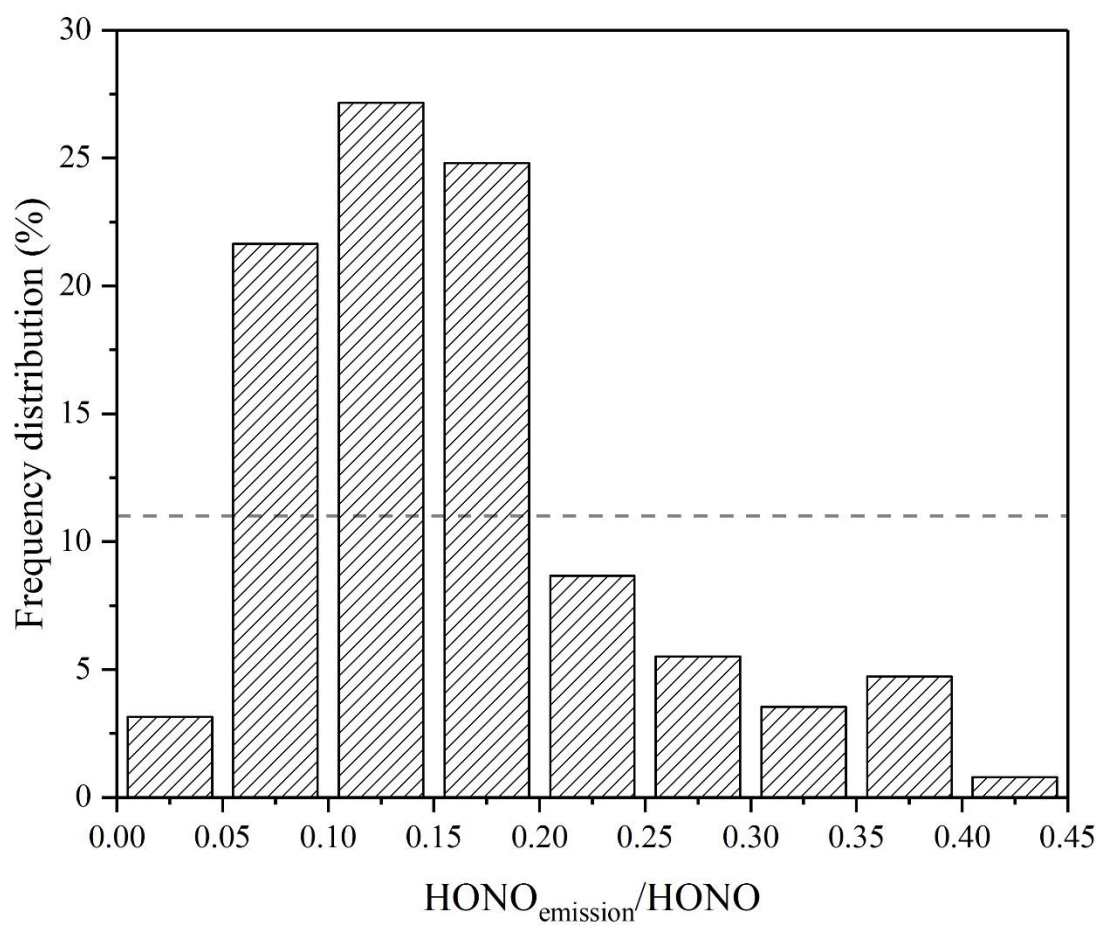
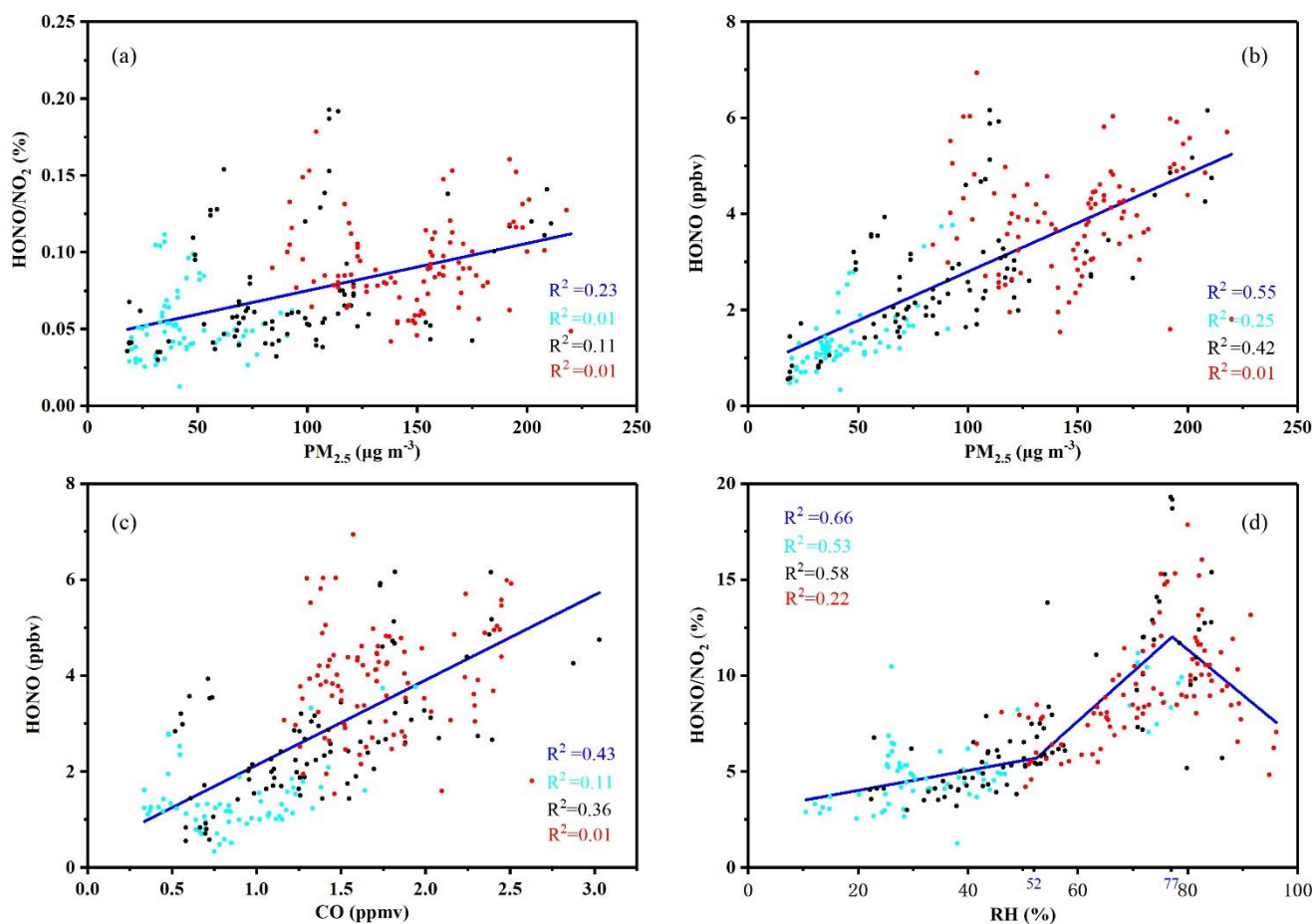**Fig. 3**. Diurnal variations of HONO during the measurement.

Fig. 4. Diurnal variations of HONO, NO, NO$_2$, O$_3$, HONO/NO$_2$, and HONO/NO$_X$. The blue points and lines represented the CD period; the black points and lines represented the PD period; the red points and lines represented the SPD period.
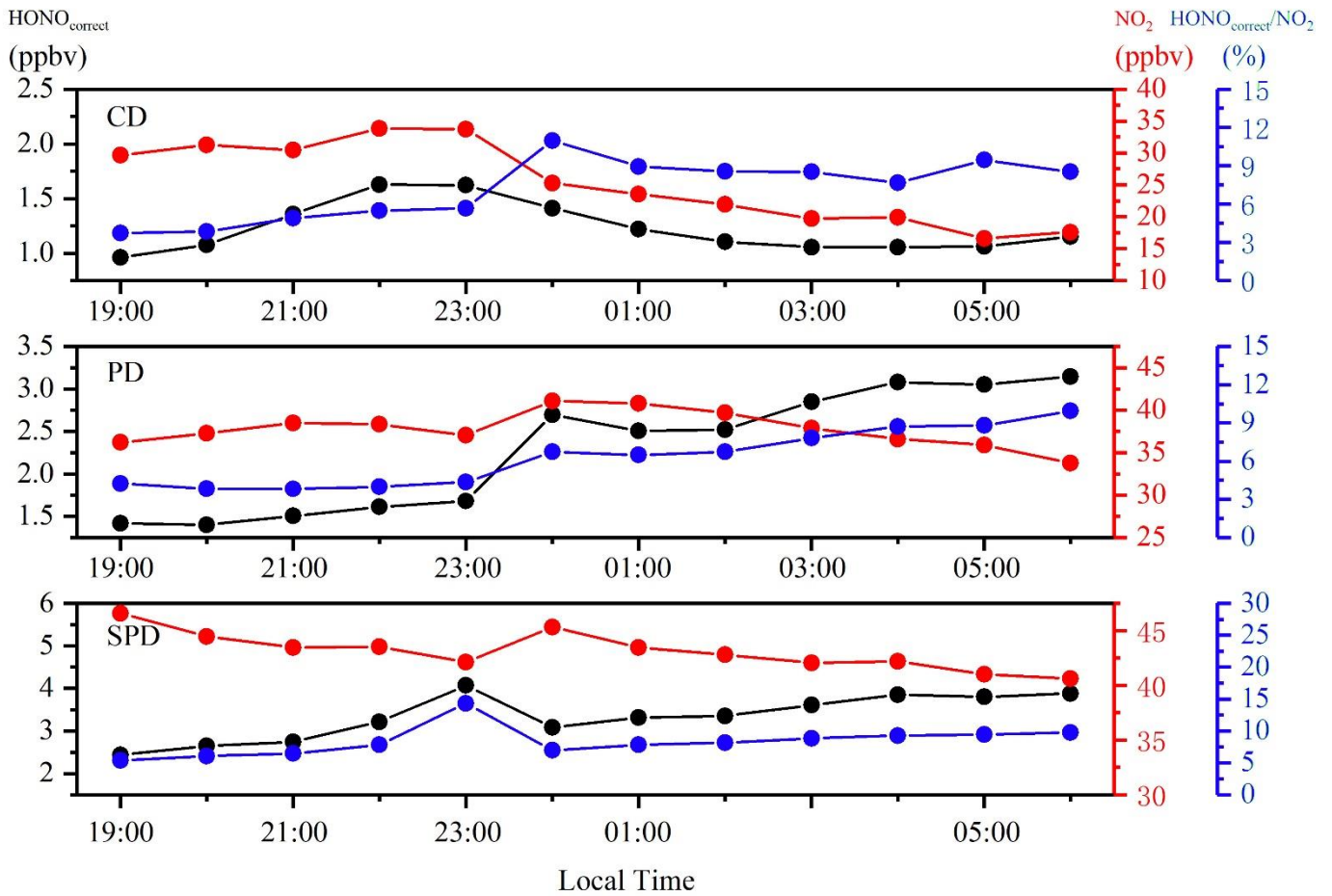
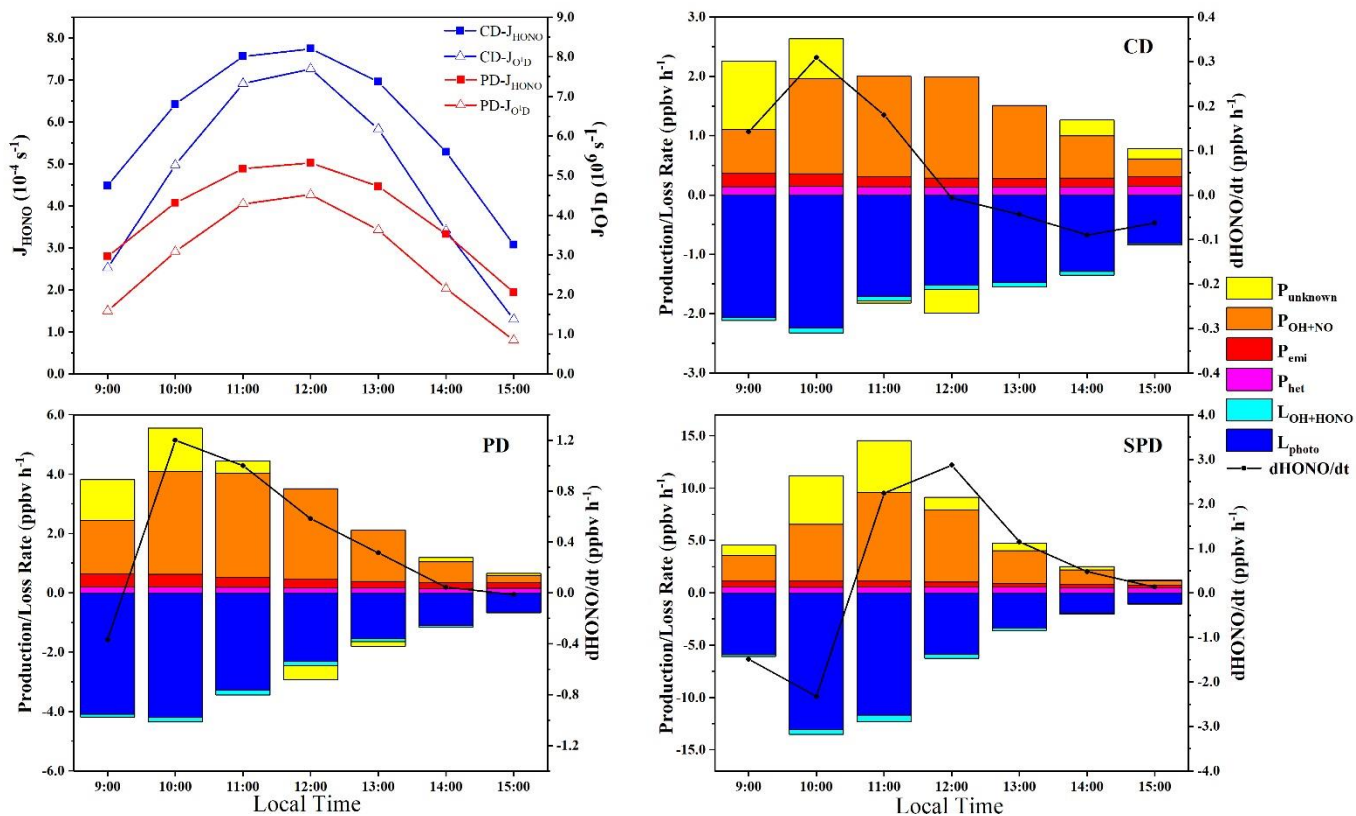**Fig. 5.** Nocturnal variations of P^{net}_{OH+NO}, HONO and NO during CD, PD and SPD periods.

Fig. 6. Percentage distribution of the nighttime $HONO_{emission}/HONO$. (The dotted line represents the average of $HONO_{emission}/HONO$.)

Fig. 7. Nighttime correlation studies between PM$_{2.5}$ and HONO/NO$_2$, PM$_{2.5}$ and HONO, CO and HONO, RH and HONO/NO$_2$ during the entire measurement period, CD, PD, and SPD periods. The blue represented the full measurement period; the light blue represented CD period; the black represented PD period; the red represented SPD period.

Fig. 8. Nocturnal variations of HONO$_{correct}$, NO$_2$, and HONO$_{correct}$/NO$_2$ in CD, PD and SPD periods.

Fig. 9. The average profiles of J_{HONO} and J_{O^1D} concentrations during the daytime, and production and loss rate of the daytime HONO in CD, PD and SPD periods.

Table Captions:

Table 1. Data statistics of HONO, $PM_{2.5}$, NO_2, NO, NO_X, $HONO/NO_2$, $HONO/NO_X$, O_3, CO, T, RH, and WS during the measurement period, mean value $\pm$ standard deviation.

Table 2. Comparisons of the daytime and nighttime HONO level, $HONO/NO_2$, and $HONO/NO_X$ mean values in Zhengzhou and other sites around the world.

Table 1.

Data statistics of HONO, $PM_{2.5}$, NO_2, NO, NO_X, $HONO/NO_2$, $HONO/NO_X$, O_3, CO, T, ==RH, and WS== during the measurement period, mean value ± standard deviation.

Trace gases	CD			PD			SPD			Total days
	Day	Night	All	Day	Night	All	Day	Night	All	
$PM_{2.5}$ ($\mu g\ m^{-3}$)	37 ± 15	41 ± 17	39 ± 16	80 ± 32	93 ± 46	87 ± 40	148 ± 29	147 ± 33	147 ± 31	91 ± 54
HONO (ppbv)	0.9 ± 0.7	1.4 ± 0.7	1.1 ± 0.7	1.9 ± 1.7	2.7 ± 1.3	2.3 ± 1.5	3.5 ± 2.7	4.0 ± 1.1	3.7 ± 2.1	2.5 ± 1.9
CO (ppmv)	1 ± 0.3	1 ± 0.3	1 ± 0.3	1 ± 0.4	1 ± 0.6	1 ± 0.5	2 ± 0.6	2 ± 0.4	2 ± 0.5	1 ± 0.6
NO (ppbv)	18.4 ± 39.3	15 ± 34.3	16.7 ± 36.8	20.3 ± 26.2	30.7 ± 33.6	25.5 ± 30.4	40.8 ± 50.8	64.3 ± 82.1	52.5 ± 68.9	31.8 ± 51.4
NO_2 (ppbv)	23 ± 13	26 ± 13	25 ± 13	29 ± 9	38 ± 10	33 ± 11	40 ± 11	43 ± 10	42 ± 11	33 ± 14
O_3 (ppbv)	21.4 ± 11.5	13.8 ± 10.0	17.6 ± 11.4	17.4 ± 11.9	8.9 ± 8.1	13.1 ± 10.9	15.6 ± 14.2	7.9 ± 7.1	11.8 ± 11.8	14.2 ± 11.7
$HONO/NO_2$ (%)	4.2 ± 3.6	5.3 ± 2.2	4.7 ± 3.1	6.8 ± 5.8	7.4 ± 3.9	7.1 ± 4.9	9.0 ± 7.7	9.8 ± 5.8	9.4 ± 6.8	7.6 ± 6.4
$HONO/NO_X$ (%)	3.3 ± 2.7	6.0 ± 5.6	4.5 ± 4.5	4.4 ± 2.5	4.6 ± 1.7	4.5 ± 2.1	5.3 ± 3.4	5.8 ± 4.7	5.6 ± 4.1	4.9 ± 3.8
RH (%)	30 ± 21	36 ± 20	33 ± 21	44 ± 17	54 ± 18	49 ± 18	64 ± 18	73 ± 13	68 ± 16	50 ± 24
WS ($m\ s^{-1}$)	0.8 ± 1.0	0.5 ± 0.7	0.7 ± 0.9	1.1 ± 1.4	0.6 ± 0.9	0.9 ± 1.2	0.4 ± 0.7	0.3 ± 0.6	0.4 ± 0.7	0.6 ± 0.9
T (℃)	4.3 ± 4.6	2.7 ± 3.6	3.5 ± 4.2	3.7 ± 3.3	2.6 ± 3.1	3.1 ± 3.2	4.6 ± 3.2	2.9 ± 2.1	3.8 ± 2.8	3.5 ± 3.5

Table 2.

Comparisons of the daytime and nighttime HONO level, HONO/NO$_2$, and HONO/NO$_X$ mean values in Zhengzhou and other sites around the world.

Date (Site)	Instrument	HONO (ppbv)			HONO/NO$_2$ (%)		HONO/NO$_X$ (%)		Reference
		Day	Night	N/D	Day	Night	Day	Night	
Oct.–Nov. 2014 (Beijing, urban)	LOPAP (long path absorption photometer)	0.9	1.8	2.0	2.6	4.6	1.7	2.2	Tong et al., 2015
Feb.–Mar. 2014 (Beijing, urban)	LOPAP	1.8	2.1	1.2	3.8 (Severe haze)	4.3	2.5	2.5	Hou et al., 2016
		0.5	0.9	1.8	7.8 (Clean)	3.0	5.1	2.4	
Jul. 2006 (Guangzhou, rural)	LOPAP	0.2	0.9	4.5	1.0	2.5	4.3	4.5	Li et al., 2012
Jul. 2014–Aug. 2015 (Xi'an, urban)	LOPAP	0.5	1.6	3.2	3.3	6.2			Huang et al., 2017
Aug. 2010–Jun. 2012 (Shanghai, urban)	Active DOAS	0.8	1.1	1.4	4.2	4.5			Wang et al., 2013
Jul. 2009 (Paris, urban)	wet chemical derivatization technique-HPLC/UV-VIS detection	0.1	0.2	2.0	3.3	2.5			Michoud et al., 2014
Jan. 2019	AIM	2.2	2.8	1.3	6.8	8.5	4.4	5.5	This study